NEW BIMODAL SCATTERED RADIATION TOMOGRAPHIC IMAGING WITH ATTENUATION AND ELECTRON DENSITY CORRECTION ALGORITHM

Gaël Rigaud[1,2]*, Rémi Régnier*[2,⋆] *and Maï K. Nguyen*[2]

[1] Institute for Applied Mathematics, Saarland University, D-66041 Saarbrücken, Germany
[2]ETIS - ENSEA/Univ. Cergy-Pontoise/CNRS, 95000 Cergy-Pontoise, France
{gael.rigaud,remi.regnier}@ensea.fr, mai.nguyen-verger@u-cergy.fr

ABSTRACT

Bimodal medical imaging, which combines two non-invasive techniques to explore two different aspects (e.g. function and morphology) of an organ, has emerged as a major clinical imaging modality nowadays. The gained information as compared to single modality imaging is overwhelmingly useful for diagnostics and therapy planning. Up to now all bimodal techniques make use exclusively of primary radiation. In this work, we describe a new bimodal imaging concept based solely on the exploitation of scattered radiation. Following a presentation of its theoretical basis, we discuss the modelings of measurements and inversion formulae used for image reconstruction. Thus an attenuation and electron density correction algorithm inspired of the Iterative Pre-Correction algorithm (IPC) is proposed. Simulation results demonstrate convincingly the feasibility and efficiency of this new bimodal imaging modality.

Index Terms— Biomedical imaging, Computed tomography, Reconstruction algorithms.

1. INTRODUCTION

At present, we observe that three major medical imaging modalities (Computed tomography : CT, Single-photon emission computed tomography : SPECT, Positron emission tomography : PET) make use only of primary (or non scattered) radiation beams whereas scattered radiation is considered as noise and then is routinely eliminated or at least compensated for [1]. Thus, it is natural to ask whether a bimodal imaging system can be built on the exploitation of scattered radiation. Imaging with scattered radiation has a long story since it has been initiated in the 50's, at a time when research on SPECT, PET and CT imaging has just started. The central idea of scattered radiation imaging is based on Compton scattering effect. Different approaches were suggested by various groups and the concept of Compton scatter tomography (CST) has emerged as a key idea for building a CST scanner, which could be as efficient as primary radiation scanners [2, 3, 4, 5, 6]. The concept was further promoted by a pioneering work performed by Norton in 1994.

The mathematical basis of CT, SPECT and PET imaging is contained in the classical Radon transform. Image formation is described by straight line integrals respectively of the attenuation map, the gamma-ray activity density and the positron activity density of the object under investigation. However scattered radiation imaging requires more general Radon transforms. For CST by transmission, the data basically consists of integrals of the matter electron density along circular arcs joining an external point source to a point-like detector. Each circular arc corresponds to a given detected energy, which through the Compton relation means a fixed scattering angle. This is why these circular arcs are called *isogonic* arcs. One deals no longer with the classical Radon transform but with the circular-arc Radon transform (CART). Fortunately, Cormack has already derived the inverse transform [7, 8] whereas Norton has given a variant of the inverse formula [9]. We shall use the Norton CST modality as one component of our bimodal scatter imaging system. The second imaging component is the V-line emission imaging (VEI). The object is now converted into a radiating object, for example by injection of a radiopharmaceutical, and restricted to a two-dimensional slice. Then using a collimated gamma camera, the data collected at each pixel for a given scattered energy is proportional to the sum of all the integrals of matter gamma-ray activity density along V-lines (broken straight lines with the form of a capital letter V standing vertically), which have an axis parallel to the collimator axis and an opening angle given by the detected energy through the Compton relation. In fact, the V-line is just a two-dimensional cone and the relevant Radon transform is called the Compounded V-line Radon transform (CVRT) [10]. As the CVRT is shown to be invertible, we can combine VEI and Norton CST into an original bimodal scatter imaging system, see Fig. 1.

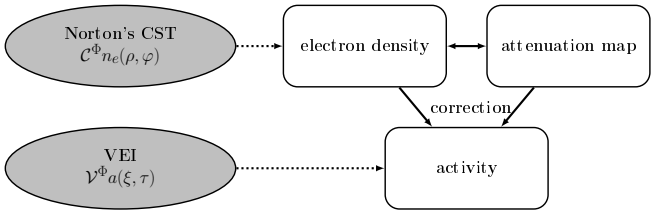

Fig. 1. Concept of a novel bimodal system

In general the two components of a bimodal imaging system deliver complementary information. For example, in a SPECT/CT system the attenuation map obtained by CT scanning is used to correct the SPECT data prior or during the reconstruction of the activity density of the object. In the proposed new scatter radiation bimodal imaging system, the object electron density is obtained by Norton's CST, from which the object attenuation map is deduced. These maps (attenuation and electron density) are then used to correct the VEI data before correctly reconstructing the object activity density. Finally, making available the two characteristics of matter, namely its electron density and its gamma-ray activity density, morphologic and functional information can be deduced simultaneously by this bimodal imaging system. To demonstrate the performance of this imaging system, it is necessary to implement the algorithms and evaluate them using numerical simulations of various phantoms.

⋆ Rémi Régnier is supported by DGA

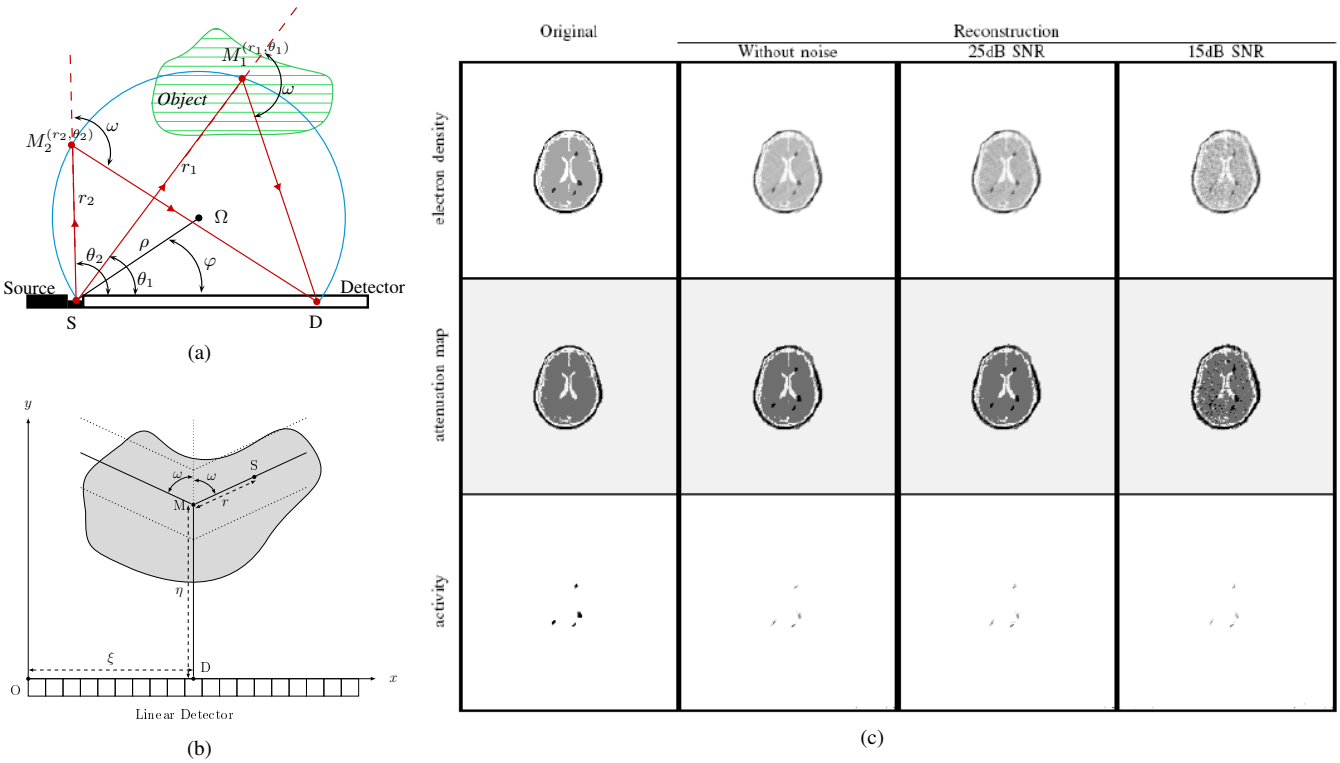

Fig. 2. Principle of Norton's CST modality (a) and of the VEI (b), their associated Radon transform and parameters setup. (c) Different reconstructions of the electron density map, attenuation map and activity map for different SNR. Reconstructions are obtained using the proposed correction algorithm and in the presence of a Poisson noise process.

Section 2 recalls the mathematical modeling of image formation in Norton's CST (by CART) and in VEI (by CVRT) with the inversion formulae. Then we establish a more realistic modeling by taking into account scattering and attenuation factors in section 3. In section 4, we present the correction algorithm for both Norton's CST and VEI in the context of the bimodal approach. Computers simulations and preliminary results described in section 5 demonstrate reasonably the feasibility and efficiency of this novel bimodal scatter imaging system. A conclusion closes the paper with some open research perspectives.

2. SCATTERED RADIATION IMAGING AND RELATED RADON TRANSFORM

The working principle of Norton's CST modality [9] is given in Fig. 2(a). In an idealized context, in order to convey the basic idea, a point-like source $\mathbf{S}$ emits primary radiation towards an object, of which $\mathbf{M}$ is a scattering site (running point). Also a point-like detector $\mathbf{D}$ moves along an Ox-axis and collects, at given energy E_ω, scattered radiation from the object. The physics of Compton scattering requires that the registered radiation flux density at site $\mathbf{D}$ is due to the scattering contribution of all scattering sites $\mathbf{M}$ lying on an arc of circle from $\mathbf{S}$ to $\mathbf{D}$ subtending an angle $(\pi - \omega)$, where ω is the scattering angle corresponding to the outgoing energy E_ω, as given by the Compton relation.

The photon flux density at site $\mathbf{D}$ can be mathematically modeled as

$$\mathcal{C}n_e(p,\varphi) = p \int_0^{\pi} d\theta \int_0^{+\infty} dr\; n_e(r,\theta)\, \delta\left(r - p\cos(\theta-\varphi)\right)\ . \tag{1}$$

where $\delta\left(r - 2\rho\cos(\theta-\varphi)\right)$ is the one-dimension Dirac delta function concentrated on the circle of center Ω and radius ρ going through the source site $\mathbf{S}$, see Figure 2(a). $\mathcal{C}n_e(p,\varphi)$ is the Radon transform of the object electron density $n_e(r,\theta)$ on arcs of circle passing through a fixed point $\mathbf{S}$ of equation $r = p\cos(\theta-\varphi)$.

Under this form, inversion via circular harmonic components is worked out by A M Cormack as follows [7, 8]. Let $f_l(r)$ be the Fourier angular components of a function $f(r,\theta)$ given by

$$f_l(r) = \frac{1}{2\pi}\int_0^{2\pi} f(r,\theta)e^{-il\theta}d\theta\ . \tag{2}$$

Following A M Cormack, one can write down the inverse formula as

$$n_{el}(r) = \frac{1}{\pi r}\int_0^{r} \frac{e^{-|l|\cosh^{-1}(r/p)}}{\sqrt{(\frac{r}{p})^2-1}}\ \left(\mathcal{C}n_{el}\right)'(p)dp - \frac{1}{\pi r}\int_r^{+\infty} U_{|l|-1}(r/p)\ \left(\mathcal{C}n_{el}\right)'(p)dp \tag{3}$$

where f' stands for the derivative of f and $U_{l-1}(\cos x) = \sin lx/\sin x$ is the Tchebychev polynomial of second kind. $n_e(r,\theta)$ is then reconstructed through its Fourier expansion with the circular harmonic components $n_{el}(r)$.

The working principle of the VEI and its associated CVRT for an idealized context (without attenuation and for constant electronic density n_e) [10] are given in Fig. 2(b). A two-dimensional object contains a non-uniform radioactivity source distribution emitting primary photons of energy E_0. A collimated linear static detector collects, at given energy E_ω, scattered radiation from this object in a direction parallel to that of the collimator holes. The physics of Compton scattering requires that the registered radiation flux density $g(\mathbf{D})$ at site $\mathbf{D}$ is due to the sum of the contribution of all emitting object point sources located on two half-lines starting at a site $\mathbf{M}$ and making an angle ω with the collimator axis direction, for all possible $\mathbf{M}$ along the axis of the collimator at $\mathbf{D}$.

Let $a(x,y)$ be an activity density function, then $\mathcal{V}a(\xi,\omega)$ the measured photon flux density at $\mathbf{D}$ under a scattering angle ω is given by

$$\mathcal{V}a(\xi,\omega) = \int_{\mathbb{R}^2_+} \frac{dr d\eta}{4\pi^2 r\eta}\, a(\pm, \eta + r\cos\omega) \tag{4}$$

where $a(\pm,.) = a(\xi + r\sin\omega,.) + a(\xi - r\sin\omega,.)$.

Eq. (4) is the compounded $\mathcal{V}$-line Radon transform (CVRT) of $a(x,y)$ and decribes image formation in the emission imaging modality from the scattered radiation [10].

The inversion of the CVRT has been established in [10] and the inversion formula is :

$$a(x,y) = \int_{-\infty}^{+\infty}\int_{-\infty}^{+\infty} \frac{e^{2i\pi q(y-z)} h(x,z)}{\gamma + i\frac{\pi}{2} sgn(q) - \ln(2\pi|q|)} dz dq \tag{5}$$

with

$$h(x,z) = \frac{z}{\pi}\int_0^{\frac{\pi}{2}} p.v.\left(\int_{\mathbb{R}} \frac{\mathcal{V}\tilde{a}(u,\omega)}{u - x\cos\omega \pm z\sin\omega} du\right)\frac{d\omega}{\cos\omega} + \frac{z}{\pi}\int_0^{\infty} p.v.\left(\int_{\mathbb{R}} \frac{\mathcal{V}a(\xi,-\tau)}{\xi - x \pm z\tau} d\xi\right) d\tau\,, \tag{6}$$

putting $\omega = \arctan\tau$, $u = \xi\cos\omega$ and $\mathcal{V}\tilde{a}(u,\omega) = \mathcal{V}a(\xi,\tau)$. As this expression can be rewritten as a simple backprojection over corresponding broken lines convolved with a filter, it does not need a specific computational regularisation.

3. MODELING WITH SCATTERING AND ATTENUATION FACTORS

In fact the interaction ray/matter must be taken into account to deal with a more realistic modeling of our imaging system. Indeed when a photon flux crosses over some matter, it is submitted to attenuation.

Moreover the Compton differential cross section, $\sigma^c(\omega)$, must be added in our modelings since here we use the scattered radiation as imaging agent. However this factor is a function of the scattering angle, ω, and so doesn't represent an obstacle for the inversion procedure.

When Compton scattering and attenuation are taken into account, eq. (1) becomes

$$\mathcal{C}^\phi n_e(\rho,\varphi) = \int_0^\pi d\theta \int_0^\infty dr\; n_e(r,\theta)\; w(r,\theta;\rho,\varphi)\; w_{att}(r,\theta;\rho,\varphi)\; \delta\left[r - 2\rho\cos(\theta-\varphi)\right]\,, \tag{7}$$

with

- $w_{att}(r,\theta;\rho,\varphi) = \exp\left(-\int_0^r \mu_0(t\cos\theta, t\sin\theta)dt - \int_0^{\frac{r\sin\theta}{\sin(\theta-\omega)}} \mu_\omega(r\cos\theta + t\cos(\omega-\theta), r\sin\theta + t\sin(\omega-\theta))dt\right)$,
- $w(r,\theta;\rho,\varphi) = \dfrac{r\,\sigma^c(\omega)}{4\pi\,(2\rho)^3\,\sin^2\theta}$.

(8)

This equation describes image formation in the transmission imaging modality from the scattered radiation.

In the same way we can propose a more realistic image formation equation in the case of the VEI

$$\mathcal{V}^\phi a(\xi,\omega) = \int_{-\infty}^{+\infty}\frac{d\eta}{2\pi\eta}\int_{-\infty}^{+\infty}\frac{dr}{2\pi r}\, Y(r)Y(\eta)\,\sigma^c(\omega)\, n_e(\xi,\eta)\; e^{-\int_0^\eta \mu_a^k(\xi,\eta')d\eta'}\left(e^{-\int_0^r \mu_a^0({\xi'}_+,\eta+r'\cos\omega)dr'}\; a(\xi_+,\eta+r\cos\omega) + e^{-\int_0^r \mu_a^0({\xi'}_-,\eta+r'\cos\omega)dr'}\; a(\xi_-,\eta+r\cos\omega)\right)\,, \tag{9}$$

with ${\xi'}_\pm = \xi \pm r'\sin\omega$ and $Y(x)$ is the Heaviside unit step function.

Taking into account the attenuation factor makes the presented above inversion procedures impossible for CART and CVRT. We still don't know a way to invert these two attenuated Radon transforms. Therefore we propose to proceed to the inversion by an iterative correction.

4. CORRECTION ALGORITHM DESCRIPTION

Numerous methods were proposed to correct for photon attenuation such as the Generalized Chang Correction (GCC) algorithm which corrects the reconstructed image in the image space or Iterative Pre-Correction (IPC) which corrects the data in the projection space, see [12]. Nevertheless these algorithms require the knowledge of the attenuation map. This information is not available in our case since we aim to recover the attenuation map from the electron density. To avoid such assumption, we propose an alternative generalized (in the sense that it can be applied both for CART and CVRT) IPC algorithm in which the attenuation map is obtained iteratively from the electron density assuming that we know the medium and its corresponding total cross-section.

We denote by T the operator $\mathcal{C}$ (resp. $\mathcal{V}$) and by $(\mathcal{X},\mathcal{Y})$, the measurable space $(\mathbb{R}^+\times[0,\pi], \mathbb{R}^+\times[0,2\pi[)$ (resp. $(\mathbb{R}^+\times\mathbb{R}^+, \mathbb{R}^+\times[0,\pi])$). Assuming that the studied image f, can be reconstructed from its measurement Tf, the following recurrence relation converges towards f

$$f^{n+1} = f^n + d^{-1}T^{-1}\circ T^\Phi\,(f - f^n) \quad \text{with} \quad f^0 = 0\,. \tag{10}$$

where n is the iteration number, T^ϕ stands for a more realistic image formation (see eqs (7) and (9)) and d is the maximum value of the kernel of T^ϕ. This relation expresses our suited IPC algorithm.

Indeed for a realistic image (activity) reconstruction based on the inverse CVRT (eq. (5)), the emission data acquired in VEI needs to be corrected by inhomogeneous electron density and attenuation.

The principle is then to reconstruct the electron density through a correction of the attenuation factor in the Norton's CST. In the context of medical applications, we can use a prior information about the studied image. Thus we assume that the studied organ (in terms of attenuation) is composed of known substances. As we don't know the attenuation map, we approximate it from the electron density at each step. Thus thanks to the following relation

$$\mu_E(\mathbf{M}) = \sigma_E(\mathbf{M}) \cdot n_e(\mathbf{M}), \tag{11}$$

with $\mu_E(\mathbf{M})$, the linear attenuation factor for a radiation of energy E at $\mathbf{M}$, $\sigma_E(\mathbf{M})$ the total cross-section of the matter at $\mathbf{M}$ for a radiation of energy E and $n_e(\mathbf{M})$ the electron density at $\mathbf{M}$, we can process to a K-means clustering to deduce an approximation of the attenuation map from the electron density. We can then update the distorsion kernel which defines the operator $\mathcal{C}^\phi$ and apply a correction of the attenuation factor, see Algorithm 1.

When the electron density and the non uniform attenuation map are established, eq. (9) gives the real emission data, *i.e.* the image formation of the activity density of the object. However such an attenuated V-line Radon transform does not possess an inverse at hand. It is necessary to correct the non constant electron density and the non uniform attenuation in the emission data before recovering the activity map by eq. (5). This procedure is iteratively carried out until convergence is reached. (see Algorithm 2). The parameter ϵ is an object-dependent threshold.

In both algorithms, N^n, S^n, M^n, A^n are the corresponding matrices of $n_e(.), \sigma_E(.), \mu_0(.), a(.)$ at iteration n and G is respectively the original data for CART and CVRT.

At last we obtain an approximated reconstruction of three informations of the studied medium : the electron density, the attenuation map and the activity, through a novel bimodal system based on scattered radiation. In the next section, we present simulation results.

Algorithm 1 μ_0 correction algorithm for CART

Input G (Norton's CST data), d and T^{-1}
$G \leftarrow G/d$
$N^1 \leftarrow T^{-1}(G)$
$S^1 \leftarrow$ K-mean algorithm on N^1 %% total cross-section
$M^1 \leftarrow S^1 \times N^1$
T^ϕ is updated
while $e^{n-1} - e^n > \epsilon$ **do**
  $G^n \leftarrow T^\phi(N^n)$
  $N^{n+1} \leftarrow N^n + d^{-1}T^{-1}(G^n - G)$
  $S^n \leftarrow$ K-mean algorithm on N^n
  $M^n \leftarrow S^n \times N^n$
  T^ϕ is updated
  $n \leftarrow n + 1$
end while
return N^n, M^n %% n_e and μ_0

5. SIMULATION RESULTS

In our experiments, we performed simulations on a computerized brain phantom, which is essentially composed of four substances such as air, water, brain and bone.

Moreover we include simulated lesions in the brain with an activity equal to 13 MBq. The HU value (Hounsfield unit) is set to 50.

The scattering medium is discretized with 256×256 pixels. We consider the number of detector positions N_x and the number of

Algorithm 2 n_e and μ_0 correction algorithm for CVRT

Input G (VEI data), d, T^ϕ and T^{-1}
$G \leftarrow G/d$
$A^1 \leftarrow T^{-1}(G)$
while $e^{n-1} - e^n > \epsilon$ **do**
  $G^n \leftarrow T^\phi(A^n)$
  $A^{n+1} \leftarrow A^n + d^{-1}T^{-1}(G^n - G)$
  $n \leftarrow n + 1$
end while
return A^n %% (a)

energy levels N_ω. In order to have a "well-conditioned" problem, the number of projections ($N_\varphi \times N_\omega$) must be larger than the number of image pixels (256×256), see for example [11]. As the measurement space is very big (because the system doesn't work with rotation around the body), we have to take a very large number of projections, this is why we put $N_\varphi = N_\omega = 1024$.

Since photon emission follows Poisson's law, this phenomenon is one of the main causes of degradation of image quality in Compton scattering tomography [1]. Thus the projections become in both cases $g(\mathbf{t}) \sim \mathcal{P}\left(Tf(\mathbf{t})\right)$ where $\mathcal{P}$ stands for the Poisson law.

Here we present the robustness of our algorithms against the Poisson noise at two levels where SNR =$25dB$ and SNR =$15dB$. The results (see Fig. 2(c)) show representative quality of the attenuation map and the activity map obtained by this approach, even in the presence of the noise (up to $SNR = 15db$).

6. CONCLUSION AND PERSPECTIVES

The new bimodal imaging proposes an alternative to current tomographic imaging techniques. The transmission Compton tomography modality can be combined with emission Compton tomography to form a new bimodal imaging based on scattered radiation. The first CST modality characterizes the studied material by its electron density (scattering sites) and permits to reconstruct an approximate attenuation map. The second modality leads to the reconstruction of the activity distribution of the studied part of the human body. Thus the reconstructions of the electron density and of the attenuation map enable a good representation of the activity through a suited correction algorithm. This latter is shown to be efficient for the correction of non-linear factors in the context of generalized Radon transforms and is particularly suited for this kind of application.

A 3D extension of the new bimodal imaging approach is a challenging issue that remains to be explored.

7. DISCUSSION

This work follows [10, 11] in which mathematical aspects and inversion procedure are described. But in [10, 11] only the scattering aspect is presented to highlight the judicious use of the scattering radiation as imaging agent. In order to make this new bimodal concept realistic, an attenuation factor is taken into account in this paper for both transmission and emission modalities. [13] deals with the attenuation correction in SPECT using scattered data. Here our imaging system is aimed to reconstruct the heterogeneous electron density and solve the attenuation problem in emission modality from the estimation of the electron density by a transmission CST modality which appears to be new. The obtained theoretical and numerical results pave the way for a novel imaging using scattered radiation and for a new concept of high-energy resolution detectors.

8. REFERENCES

[1] H. Zaidi and K. F. Koral, "Scatter modelling and compensation in emission tomography". *Eur. J. Nucl. Med. Mol. Imaging.*, vol. 31, pp. 761-782, (2004).

[2] P. G. Lale "The examination of internal tissues, using gamma-ray scatter with a possible extension to megavoltage radiography", *Phys. Med. Biol.*, vol. 4,pp. 159-167, (1959).

[3] R. L. Clarke, E. N. Milne, G. Van Dyk, "The use of Compton scattered gamma rays for tomography", *Invest Radiol.*, vol. 11(3), pp. 225-235 (1976).

[4] G. Harding, H. Strecker, R. Tischler, "X-ray imaging with Compton scatter radiation" *Philips Tech. Rev.*, vol. 41(2), pp. 46-59 (1983).

[5] N. V. Arendtsz, E. M. A. Hussein, "Energy-spectral Compton scatter imaging - Part I: Theory and mathematics", *IEEE Transactions on Nuclear Science*, vol.42, pp. 2155-2165 (1995).

[6] H. H. Barrett and W. Swindell, "Radiological Imaging: The Theory of Image Formation, Detection, and Processing", *Academic press*, San-Diego Boston New-York, Appendix C (1981).

[7] A. M. Cormack, "The Radon transform on a family of curves in the plane", *Proceedings of the American Mathematical Society*, vol.83(2), pp. 325-30 (1983)

[8] A. M. Cormack "Radon's problem - Old and new", *SIAM - AMS Proceedings*, vol. 14, pp. 33-39 (1994)

[9] S. J. Norton, "Compton scattering tomography", *J. Appl. Phys*, vol. 76, pp. 2007-2015 (1994).

[10] T. T. Truong and M. K. Nguyen, "On new V-line radon transforms in $\mathbb{R}^2$ and their inversion", *J. Phys. A: Math. Theor.,* vol. 44,pp. 075206 (2011).

[11] G. Rigaud, M. K. Nguyen, and A. K. Louis, "Novel numerical inversions of two circular-arc Radon transforms in Compton scattering tomography", *Inv. Prob. Sci. Eng.*, doi: 10.1080/17415977.2011.653008 (2012).

[12] A. Maze, J. L. Cloirec, R. Collorec, Y. Bizais, P. Braindet, and P. Bourguet, "Iterative reconstruction methods for nonuniform attenuation distribution in SPECT". *J. Nucl. Med.*, vol. 34, pp. 1204-1209, (1993).

[13] S.C. Cade, S. Arridge, M.J. Evans and B.F. Hutton, "Attenuation map estimation without transmission scanning using measured scatter data". *Nuclear Science Symposium and Medical Imaging Conference (NSS/MIC)*, pp 2657-2663, (2011).